46th AIAA Aerospace Sciences Meeting and Exhibit
7 - 10 January 2008, Reno, Nevada

AIAA 2008-475

Boundary-Layers Integral Analysis - Heated Airfoils in Icing Conditions

Guilherme Araújo Lima da Silva*
Escola Politécnica, University of São Paulo, São Paulo, SP, 05508-900, Brazil

Otávio de Mattos Silvares†‡
Escola Politécnica, University of São Paulo, São Paulo, SP, 05508-900, Brazil
Instituto Mauá de Tecnologia, São Caetano do Sul, SP, 09580-900, Brazil

Euryale Jorge Godoy de Jesus Zerbini§
Escola Politécnica, University of São Paulo, São Paulo, SP, 05508-900, Brazil

Under icing conditions, it is necessary to heat and control the temperature of the airfoil surface at leading edge region to prevent ice formation. The thermal anti-ice system balances mainly the evaporative cooling effects, which are caused by the coupled heat and mass convection transfer, imposed by the air flow loaded with supercooled water droplets and the runback water flow around the airfoil. The most difficult and important parameter for accurate estimation of airfoil surface temperatures and water runback mass flow rates is the local convective heat transfer coefficient. This paper presents an integral analysis of momentum and thermal boundary-layers applied to heated airfoils operating in icing conditions. The objectives are to implement two different mathematical models, assess the effects of the model assumptions on the results accuracy and compare the numerical results obtained with reliable experimental data. One boundary-layer model assumes isothermal and non-permeable surface with presence of a abrupt laminar-turbulent transition. These are common assumptions adopted by previous workers. The other model, proposed by present authors in previous works, considers the boundary-layers over a non-isothermal and permeable surface with a smooth laminar-turbulent transition region. The onset and length of laminar-turbulent transition may be estimated by classic empirical correlations or just imposed. All numerical results are compared with classic and recent experimental data of two different thermal anti-iced airfoils operating in icing tunnel.

Nomenclature

B_h	heat transfer driving force
c	airfoil chord, m
c	airfoil chord, m
C_f	local friction coefficient $\tau/(1/2 \cdot \rho_e \cdot u_e^2)$
D	mass diffusivity, m^2/s
F	overall wetness factor
h_{air}	convection heat transfer coefficient, $W/(K \cdot m^2)$
i	specific enthalpy, J/kg
Le	Lewis number $c_p \cdot D_{water,air} \cdot \rho/k$
$l(\lambda)$	function of pressure gradient parameter in Eq. (9)

*M.Sc., Graduate Student, Mechanical Engineering Department, Av. Prof. Mello Moraes, 2231, AIAA Member
†Associate Professor, Mechanical Engineering Department, Av. Prof. Mello Moraes, 2231.
‡Dean, University Dean Office, Praça Mauá, 1.
§Doctor, Mechanical Engineering Department, Av. Prof. Mello Moraes, 2231.

Nu	gaseous flow local Nusselt number $(h_{air} \cdot s)/k_{air} = \mathrm{St}_{air} \cdot \mathrm{Re}_s \cdot \mathrm{Pr}_{air}$
Pr	Prandtl number $\mu \cdot c_p/k$
$\dot{q}_{lost}$	heat transfer rate lost to gaseous flow, W
Re_{Δ_2}	Reynolds number based on enthalpy thickness $u_e \cdot \Delta_2/\nu_{air}$
Re_{δ_2}	Reynolds number based on momentum thickness $u_e \cdot \delta_2/\nu$
Re_∞	Reynolds number based on airfoil chord and freestream velocity $V_\infty \cdot c/\nu_{air}$
R_t	thermal resistance, K/W
St	gaseous flow local Stanton number $h_{air}/(\rho_{air} \cdot u_e \cdot c_{p,air})$
T_{rec}	recovery temperature of an adiabatic wall, K
Tu	freestream turbulence level, $Tu = \sqrt{\frac{u'^2}{U^2}}$
U	overall heat transfer coefficient, W/(m$^2\cdot$ K)
u	boundary layer streamwise velocity, m/s
v	boundary layer normal velocity, m/s
ΔT	temperature difference between gaseous flow interface and external flow, K
δ_1	boundary layer displacement thickness, m
Δ_2	boundary layer enthalpy thickness, m
δ_2	boundary layer momentum thickness, m
λ	pressure gradient parameter

Subscripts

E	end
0	boundary layer interface with airfoil solid surface $y = 0$
lam	laminar regime
lv	liquid-vapor saturation
stag	airfoil leading edge stagnation point
stag	airfoil leading edge stagnation point
tr	transition onset
turb	turbulent regime

Superscripts

$*$	indicates the blowing effect in gaseous flow local Stanton number

I. Introduction

THE coupled convection heat and mass transfer from the heated airfoil surface to the icing environment mostly defines the thermal demand of a steady state anti-ice system operation. As observed by the present authors,[1–5] an accurate prediction of the momentum and thermal boundary-layers combined with a estimation of surface wetness factor decrease the deviation between numerical results and experimental data for temperatures and runback mass flow rate in wet, evaporative and full evaporative operational regimes.

Previous works pointed out the importance of the convective heat transfer coefficient h_{air} estimation in both airfoil ice shape prediction[6,7] and airfoil thermal ice protection system design.[1,8–11] The h_{air} coefficient affects significantly the overall heat transfer because the airfoil surface temperatures T_{wall} are maintained above the local recovery temperature T_{rec}. In such condition, far from thermal equilibrium with surrounding air stream, the temperature difference ΔT_{air} magnitude makes the overall heat transfer rate sensitive to h_{air} coefficient variations. The effects are even more considerable because evaporated mass flux depends on h_{air} through heat and mass analogy. In the wetted regions, there is an enhancement of heat transfer caused by evaporation enthalpy flux from runback water to surroundings. The mass transfer rate is also function on airfoil surface temperature and local pressure distributions. In addition, depending on T_{wall} levels, the water evaporation flux may thicken the thermal boundary layer and, in turn, decrease the h_{air} value. Therefore, the h_{air} distribution prediction is critical to an adequate the coupled heat and mass transfer estimation.

Most works found in the bibliographic research deals with boundary layer integral analysis applied to icing airfoils.[6,12–16] These papers use mathematical models that assumes laminar and turbulent flows over isothermal, fully rough icing surface with moderate pressure gradient and no evaporation effects on boundary-layer growth rate. The laminar-turbulent transition is considered to occur abruptly, i.e., the flows goes from fully laminar to fully turbulent at the onset position. The classic icing codes LEWICE,[13,17] ONERA2D[14] and TRAJICE2[15] adopt similar model or are based on Makkonen[12] formulation.

Few researchers implemented momentum and thermal boundary layer integral models for use in thermal ice protection design. Morency, Tezok and Paraschivoiu[18] developed the numerical code CANICE A that evaluates the h_{air} considering laminar flow over isothermal surface,[19] turbulent flow over smooth and non-isothermal surface[20] and abrupt laminar-turbulent transition. Same authors developed other version of the code, CANICE B, that uses only h_{air} experimental distribution directly in water and airfoil surface thermal balance equations. Only this second code represented satisfactorily the surface temperature numerical results. In his first code version, Henry's[21] applied the Makkonen[12] boundary-layer model that, in turn, is used in ONERA2D icing code.[14] Al-Khalil *et. al*[10] employed experimental data and did not evaluate h_{air} coefficient inside ANTICE numerical code. Gent *et. al*[11] reported difficulties when applying TRAJICE2 boundary layer model[6,15] to rotorcraft ice protection systems. The authors obtained overestimated results due to rough surface assumption in $h_{air,turb}$ evaluation. Therefore, they recommended more research in order to find more refined procedures for external heat transfer calculation.[11]

Other authors present the use of boundary-layer differential analysis to solve the heat mass convection over smooth and non-isothermal surfaces with a laminar-turbulent transition model based on intermittency concept. Cebeci modified his two-dimensional finite differences code[22] to simulate flow on airfoils with environmentally rough and iced surface.[23,24] Later, Fortified/LEWICE code version incorporated these techniques.[25,26] Henri[27] used a two-dimensional finite difference code to evaluate heat transfer in ice protection transient operation. In the same direction, Morency, Tezok and Paraschivoiu[28] published the CANICE FD version that evaluates h_{air} distribution with Cebeci code.[22] Croce, Beaugendre and Habashi[29] developed a conduction and convection heat transfer estimation by using finite element method.

II. Objective

This paper presents an momentum and thermal boundary-layers mathematical integral models for convection evaluation. The objectives are to implement, compare numerical results and verify accuracy of two different models: 1) classic, which assumes flow over an isothermal and non-permeable surface with presence of a abrupt laminar-turbulent transition; 2) present, which assumes flow over a non-isothermal and permeable surface with a smooth laminar-turbulent transition region based on intermittency function.

III. Airfoil Anti-ice Mathematical Model

The present paper uses the anti-ice thermal model developed by Silva, Silvares and Zerbini,[4,5] whom briefly described the mathematical model, presented some numerical code results and compared with experimental data as well as other codes results. The anti-ice system operation simulation applies the First Law of Thermodynamics to liquid water flow and solid airfoil surface together the Conservation of Mass and Momentum to liquid water flow. The wetness factor estimation, by water film breakdown and rivulets formation, was based in other work[3] plus the assumption of constant rivulets spacing.

The anti-ice simulation problem requires solution of : 1) velocity and pressure fields around the airfoil; 2) droplet trajectories; 3) momentum and thermal boundary layers to obtain the coupled heat and mass transfer over the airfoil solid surface and liquid water flow; 4) First Law of Thermodynamics to the liquid water and airfoil solid surface plus the Conservation of Mass and Momentum to the liquid water flow (film and rivulets) over the airfoil. Both flow field around airfoil and local collection efficiency data were provided by external numerical codes (1 and 2). The momentum and thermal boundary-layer are evaluated (3) in order to estimate the heat and mass transfer around airfoil over non-isothermal and transpired surfaces with a smooth laminar-turbulent transition occurrence.[4] With data from previous steps (1, 2, 3), the anti-ice mathematical model (4) is able to predict operational parameters like solid surface temperatures, runback mass flow rate and convection heat transfer coefficient distributions along the airfoil solid surface. The anti-ice thermal (4) model and boundary-layer (3) integral analysis have been developed since works of.[1,30]

The present paper presents modeling strategies for the thermal boundary-layer (3) only. The boundary-layer integral analysis described herein, non-isothermal with an intermittency-based transition, has been applied by present authors to airfoil[1–5] and turbofan engine inlet[31] thermal anti-ice numerical simulation.

IV. Heat Transfer around Thermally Protected Airfoils

The heat transfer around thermally protected airfoil operating under icing conditions is mainly affected by heat and mass convection mechanisms but also by conduction, surface wetness factor, runback water enthalpy flow and droplets impingement.

A. Momentum and Thermal Boundary-Layers

The evaluation of the convective heat transfer and friction coefficients distribution around the airfoil is performed by solving the the thermal and dynamic boundary layers equations in integral form at laminar and turbulent regimes. For the laminar to turbulent transition region, it is proposed a linear combination of turbulent and laminar results weighted by a exponential probability function.

In the present paper, both momentum and thermal boundary layer equations are simplified considering a steady state and one-dimensional flow with moderate pressure gradient over a smooth, nonisothermal and impermeable surface. These assumptions leads to Eqs. (6) and (13). Note that evaporation mass flux is neglected in those equations, however, the effect of blowing in convective heat transfer is estimated, Eqs. (1) and (2), during calculation of water liquid film and airfoil solid surface temperatures. The solution of thermal boundary layer equation provides the value of St with no blowing in order to estimate $\dot{m}''_{evap}$ and B_h so that the St^* with blowing effect is calculated.

B. Mass Transfer Blowing Effect

The heat transfer driving force of convective evaporative cooling is defined by Spalding:[32]

$$B_h = \frac{\dot{m}''_{evap}}{St^* \cdot G} \tag{1}$$

Then the effect of blowing on both laminar and turbulent convective heat transfer is accounted in thermal boundary-layer:

$$\frac{St^*}{St} = \frac{\ln(1 + B_h)}{B_h} \tag{2}$$

This is a coupled heat and mass transfer process where St^* depends on B_h, Eq. (2), that depends on both $\dot{m}''_{evap}$ and St^*, Eq. (1). The iterative calculation process only finishes when First Law of Thermodynamics is satisfied in each finite volume.

C. Water Film Breakdown and Rivulets Formation

From stagnation point to impingement region limits, the runback water is assumed to flow as a continuous film. Downstream the limits, a wetness factor is calculated by using a rivulets formation model[3] that adopts the Minimum Total Energy criteria.[33,34] It proposes four equations to find the critical film thickness, the rivulets wetness factor F_r, rivulet radius and center-to-center rivulets spacing: 1) conservation of mass in the transition between film and rivulets flow patterns in streamwise direction; 2) conservation of total energy from film to rivulet in streamwise direction; 3) rivulet total energy minimization; 4) geometrical relationships. Alike other wing anti-ice models,[10] the present model defines the overall wetness factor F as the ratio between wet and total area of finite volume:

$$F = F_r \cdot F_s \quad \text{where} \quad 0 \leqslant F \leqslant 1 \quad \text{and} \quad F = \frac{A_{wet}}{A_{total}} \quad \text{where} \quad A_{total} = A_{dry} + A_{wet} \tag{3}$$

where the wetness factor F_r is defined as the ratio between the rivulet base width and the distance between two rivulets centers λ, F_s is the ratio of streamwise wetted distance by the finite volume total distance; A_{total} is the total finite volume area. Thus, F is used to multiply A_{total} associated with water and air convective heat and mass transfer terms in First Law of Thermodynamics applied to both solid surface and runback water flow. The rivulet top curved area, as it is approximated by a segment of a cylinder, is also accounted by the model of Silva, Silvares and Zerbini.[3]

D. Overall Heat Transfer Coefficient

The overall heat transfer coefficient U is defined to take into account the effects of convective heat transfer rate across solid-liquid and liquid-gas surfaces interfaces, runback water enthalpy net flux, water droplets impingement enthalpy and evaporation enthalpy:

$$U = \frac{\dot{q}_{lost}}{1 \cdot \Delta s \cdot \Delta T} \tag{4}$$

$$\dot{q}_{lost} = R_t^{-1} \cdot 1 \cdot \Delta s \cdot \Delta T - \dot{m}_{evap} \cdot (h_{lv} + h_{water}) + \dot{m}_{imp} \cdot h_d + \dot{m}_{in} \cdot h_{in} - \dot{m}_{out} \cdot h_{out} \tag{5}$$

V. Momentum Boundary-Layer

The solution of the momentum thickness integral equations provides the C_f distribution around airfoil that is used in film and rivulet flow equations. It may be used also in the expressions to predict onset and extension of the laminar-turbulent transition. The boundary layer momentum equation can be conveniently expressed in a non-dimensional equation of momentum thickness[35]:

$$\frac{C_f}{2} = \frac{d\delta_2}{ds} + \delta_2 \cdot \left[\left(2 + \frac{\delta_1}{\delta_2} \right) \cdot \frac{1}{u_e} \cdot \frac{du_e}{ds} \right] \tag{6}$$

Based on Thwaites[36] approximation, Kays and Crawford[35] integrated the Eq. (6) in order to obtain the momentum thickness in laminar flow regime:

$$\delta_{2,lam} = \frac{0.664 \cdot \nu_{air}^{1/2}}{u_e^{2.84}} \cdot \left(\int_{s_{stag}}^{s} u_e^{4.68} \, ds \right)^{1/2} \tag{7}$$

The laminar friction coefficient $C_{f,lam}$ is evaluated in function of the pressure gradient parameter λ by the procedure developed by Cebeci and Bradshaw[22]:

$$C_{f,lam} = \frac{2 \cdot l(\lambda)}{\mathrm{Re}_{\delta_2}} \tag{8}$$

where

$$l(\lambda) = \begin{cases} 0.225 + 1.61 \cdot \lambda - 3.75 \cdot \lambda^2 + 5.24 \cdot \lambda^3 & 0 < \lambda < 0.1 \\ 0.225 + 1.472 \cdot \lambda - (0.0147 \cdot \lambda)/(\lambda + 0.107) & 0 > \lambda > -0.1 \end{cases} \tag{9}$$

For the present work, the integral equation of momentum thickness in turbulent regime, Eq. (6), is satisfactorily simplified to[35]:

$$\delta_{2,turb} = \left[\frac{0.0156 \cdot \nu_{air}^{1/4}}{u_e^{4.11}} \cdot \int_{s_{tr}}^{s} u_e^{3.86} \, ds + (\delta_{2,tr})^{5/4} \cdot (\frac{u_{e,tr}}{u_e})^{4.11} \right]^{4/5} \tag{10}$$

With momentum thickness, $\mathrm{Re}_{\delta_{2,turb}}$ is obtained to allow evaluation of $C_{f,turb}$y:

$$\frac{C_{f,turb}}{2} = 0.0125 \cdot \mathrm{Re}_{\delta_{2,turb}}^{-0.25} \tag{11}$$

VI. Thermal Boundary-Layer

A. Non-isothermal Model

At stagnation point, the local convective heat transfer is most accurately estimated by Smith-Spalding approximation:[19]

$$\mathrm{Nu}_{stag} = \left[0.246 \cdot \mathrm{Re}_{\infty} \cdot \left. \frac{d\,(u_e/V_{\infty})}{d\,(s/c)} \right|_{s=s_{stag}} \right]^{1/2} \tag{12}$$

In order to evaluate the local convective heat transfer coefficient distribution downstream the stagnation point in upper and lower airfoil surfaces, it is convenient to represent the thermal boundary layer in a non-dimensional form of enthalpy thickness:[35]

$$\mathrm{St} = \frac{d\Delta_2}{ds} + \Delta_2 \cdot \left(\frac{1}{u_e} \cdot \frac{du_e}{ds} + \frac{1}{i_0} \cdot \frac{di_0}{ds} \right) \tag{13}$$

Ambrok[20] developed an original expression in order to evaluate laminar local convective heat transfer due to a flow over non-isothermal surfaces with moderate pressure gradient:

$$\mathrm{Nu}_{lam} = 0.3 \cdot \mathrm{Re}_s \cdot \Delta T \cdot \left(\int_{s_{stag}}^{s} \frac{u_e \cdot \Delta T^2}{\nu_{air}} \, ds \right)^{-1/2} \tag{14}$$

Equation (13) is simplified in order to give the laminar regime enthalpy thickness solution:[20]

$$\mathrm{Re}_{\Delta_{2,lam}} = \frac{0.83}{\Delta T} \cdot \left(\int_{s_{stag}}^{s_{tr}} \frac{u_e \cdot \Delta T^2}{\nu_{air}} \, ds \right)^{1/2} \tag{15}$$

The local convective heat transfer in turbulent regime is evaluated by:[20]

$$\mathrm{St}_{turb} = 0.0125 \cdot \mathrm{Re}_{\Delta_{2,turb}}^{-0.25} \cdot \mathrm{Pr}^{1/2} \tag{16}$$

The turbulent enthalpy thickness is estimated by Ambrok[20] approximated solution:

$$\mathrm{Re}_{\Delta_{2,turb}} \cdot \Delta T = \left[0.0156 \cdot \mathrm{Pr}^{-1/2} \cdot \mu_{air}^{-1} \cdot \int_{s_{tr}}^{s} G \cdot \Delta T^{1.25} ds + \left(\mathrm{Re}_{\Delta_{2,tr}} \cdot \Delta T_{tr} \right)^{1.25} \right]^{0.8} \tag{17}$$

B. Isothermal Model

Classic icing codes[16] use the integral analysis of Smith-Spalding[19] to evaluate heat transfer around isothermal icing airfoils in laminar regime. Flow over isothermal surfaces is an acceptable assumption for non-heated airfoils subjected to ice formation, since the exposed ice or airfoil surface equilibrium temperatures are approximately constant. In this model, the heat transfer coefficient $h_{air,lam}$ is estimated by evaluating the laminar conduction thickness $\Delta_{4,lam}$:

$$\frac{u_e^{2.87}}{\nu} \cdot \Delta_{4,lam}^2 = 11.68 \cdot \int_{s_{stag}}^{s} u_e^{1.87} ds \qquad \text{and} \qquad \Delta_{4,lam} = \frac{k_{air}}{h_{air,lam}} \tag{18}$$

The stagnation point heat transfer is provided by Eq. (12), which is an approximation of Eq. (18) for plane stagnation similar flow, $u_e = C \cdot s$. In turbulent regime, the classic icing codes evaluate the heat transfer coefficient by assuming flow over a fully rough surface and one of heat and momentum transfer analogies. As there is no ice on the airfoil when operating an anti-ice system, the present paper assumes flow over a smooth surface and the *Colburn* analogy to estimate:

$$\mathrm{St}_{turb} \cdot \mathrm{Pr}^{2/3} = \frac{C_{f,turb}}{2} \tag{19}$$

Equation (11) provides C_f value to replace in Eq. (19).

VII. Laminar-Turbulent Transition

A. Transition Model

1. *Intermittency*

Silva, Silvares and Zerbini[4] adopted the work of Reynolds, Kays and Kline[37] that defines the laminar-turbulent transition region statistically by a mean position s_m and a standard deviation length σ. Both St and C_f within transition region are calculated by linear combination of the laminar $C_{f,lam}$ and St_{lam} with turbulent $C_{f,turb}$ and St_{turb} values.

Within the laminar-turbulent transition region, the St number is estimated by:

$$\mathrm{St}(s) = \begin{cases} \mathrm{St}_{lam}(\mathrm{Re}_s) & s < s_m - 2 \cdot \sigma \\ [1 - \gamma(s)] \cdot \mathrm{St}_{lam}(\mathrm{Re}_s) + \gamma(s) \cdot \mathrm{St}_{turb}(\mathrm{Re}_s) & s \geq s_m - 2 \cdot \sigma \end{cases} \tag{20}$$

Similarly, the linear combination procedure is also applied to friction coefficient calculation C_f, i.e., the $\mathrm{St}(s)$ is replaced by $C_f(s)$ in Eq. (20). The turbulent flow probability $\gamma(\mathrm{Re}_s)$ is evaluated by:

$$\gamma(\mathrm{Re}_s) = \int_{-\infty}^{\mathrm{Re}_s} \left(\frac{1}{\mathrm{Re}_s} \cdot \sqrt{2 \cdot \pi} \right) \cdot \exp\left(- \frac{\mathrm{Re}_s - \mathrm{Re}_{s_m}^2}{2 \cdot \mathrm{Re}_\sigma^2} \right) d(\mathrm{Re}_s) \tag{21}$$

Alike Narasimha,[38] the present paper assumes that the virtual origin of turbulent boundary coincides with the transition onset, where the turbulent spots start to appear. Thus, γ, $\delta_{2,turb}$ and $\Delta_{2,turb}$ start to be different than zero at transition onset s_{tr}. The virtual origin of boundary-layer occurs at same position of turbulent breakdown, where the turbulent spots starts to appear.

2. *Onset and Extension Prediction*

Abu-Ghannam and Shaw[39] developed empirical correlations to predict the beginning and the end of the transition region. The correlations are based in experimental data obtained in experiments with a smooth flat plate under various freestream velocity and turbulence level.

The transition onset position is given by the Eq. (22).

$$Re_{\delta_2,tr} = 163 + \exp\left(F(\lambda) - \frac{F(\lambda)}{6.91} \cdot Tu \right) \tag{22}$$

where $F(\lambda)$ is given by Eq. (23a) for $\lambda < 0$ and by Eq. (23b) for $\lambda > 0$:

$$F(\lambda) = 6.91 + 12.75 \cdot \lambda + 63.64 \cdot \lambda^2 \tag{23a}$$

$$F(\lambda) = 6.91 + 2.48 \cdot \lambda - 12.27 \cdot \lambda^2 \tag{23b}$$

The end of the transition region is also given by a correlation of the Re_{δ_2}:

$$Re_{\delta_2,E} = 540 + 183.5 \cdot \left(Re_L \cdot 10^{-5} - 1.5 \right) (1 - 1.4\lambda) \tag{24a}$$

$$Re_L = 16.8 \cdot (Re_{s,tr})^{0.8} \tag{24b}$$

In order to be coherent with Reynolds, Kays and Kline[37] intermittency formulation and previous works,[4] the present paper adopts the onset transition position as $s_{tr} = s_m - 2 \cdot \sigma$ and the end transition region position as $s_E = s_m + 2 \cdot \sigma$.

B. Abrupt Model

As reported by Wright, Gent and Guffond[16] , the classic icing codes assume that the laminar-turbulent transition region has a very short length, i.e., the flow goes from laminar to turbulent regime almost instantaneously. However, Pimenta[40] as well as Bragg, Cumming and Henze[41] observed no evidences of abrupt transition occurence in flow over fully rough flat plates or airfoils. Stefanini *et al.*[7] demonstrated that transition parameters region variation, such as onset and length, affects ice shape significantly for the cases

analyzed. Moreover, classic NACA research[8] and U.S. Air Force manual[9] concluded that laminar-turbulent transition is also important in thermal ice protection design. However, the assumption of an abrupt laminar-turbulent transition is commonly adopted by aerospace engineers and researchers in anti-ice system numerical simulation.

In abrupt model, it is assumed that enthalpy thickness Δ_2 is a continuous function at beginning of transition region location. Therefore, with value of Eq. (15) at transition onset and assumption of $\Delta_{2,tr} = \Delta_{2,lam} = \Delta_{2,turb}$. Due to same reason, $\delta_{2,tr} = \delta_{2,lam} = \delta_{2,turb}$ and the Eq. (7) provides the initial condition for the integral in Eq. (10) at transition onset position s_{tr}.

VIII. Selected Experimental Cases

A. NACA Airfoil Anti-ice tests

Gelder and Lewis[8] conducted one of the first investigations of the heat transfer from airfoil in clear air and icing in closed circuit NACA Lewis icing tunnel. The tests used a 1.839 m span by 2.438 m chord NACA 65_2-0016 airfoil that was adopted previous research[42] in ice protection flight experiments under similar electrical heating power distribution and icing conditions. The authors observed a forward movement of laminar-turbulent transition induced by water impingement and freestream turbulence level that was higher in tunnel than flight. Other important experimental evidence noticed was the heating and temperature distributions affects the measured convective heat transfer coefficient significantly. The present paper uses the NACA test case 8 under icing and clear air conditions. The liquid water content, LWC, median volumetric diameter along other icing tunnel and airfoil configuration are presented in Table 1.

Table 1: Anti-ice Test Conditions for Mathematical Models Benchmarking

	Al-Khalil *et al.*[10]		Gelder and Lewis[8]	
Parameter	22A	67A	8 icing	8 clear air
V_∞, m/s	44.7	89.4	73.8	73.8
T_{tot}, °C	-7.6	-21.6	-6.1	-6.1
LWC, g · m^{-3}	0.78	0.55	0.5	-
MVD, μm	20	20	11	-
α	0°	0°	0°	0°
airfoil	NACA 0012	NACA 0012	NACA 65_2-0016	NACA 65_2-0016
chord	0.914 m chord	0.914 m chord	2.438 m chord	2.438 m chord

B. Recent Airfoil Anti-ice tests

Al-Khalil *et al.*[10] performed anti-icing experiments at closed circuit Icing Research Tunnel at NASA Glenn Research Center facilities (former NACA Lewis), Cleveland, Ohio, USA, to measure surface temperature and overall heat transfer coefficient distributions. The test purpose was to validate NASA'S ANTICE numerical code results. The airfoil tested was 1.828 m span by 0.914 m chord NACA 0012 profile with electronically controlled heaters. Each heater element in streamwise direction had one thermocouple, one thermoresistor sensor and one heat flux gauge installed. Two tests cases from Al-Khalil *et al.*[10] experimental data set are used herein: case 22A, that is an evaporative condition with runback ending upstream the impingement limits; and 67A, that is a partial evaporative case with more water running around leading edge. Table 1 presents the experimental conditions for both cases.

IX. Results

The mathematical models listed in Table 2 were implemented and incorporated in anti-ice numerical code of Silva, Silvares and Zerbini.[3,4] The results of each model were compared with classic and recent

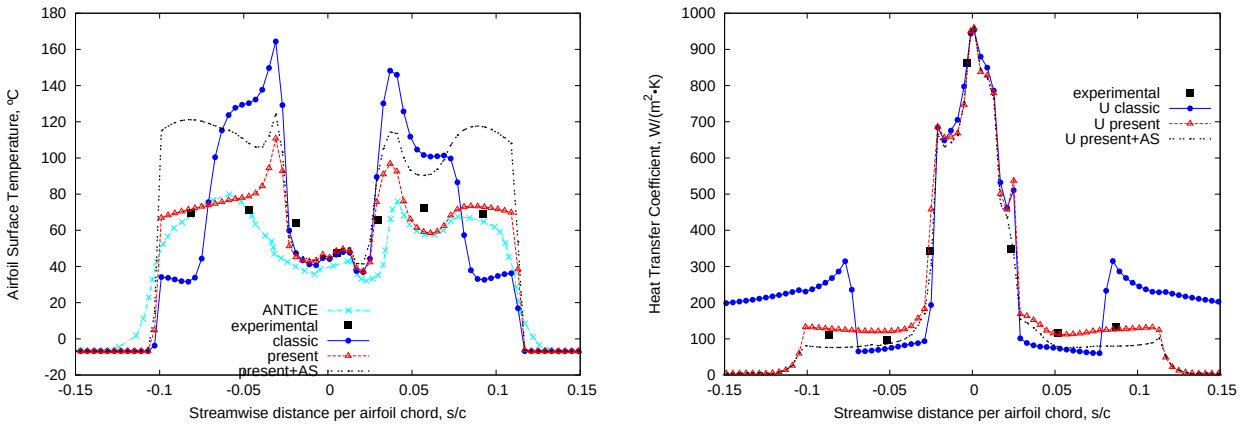

(a) Surface Temperature

(b) Overall heat transfer coefficient

Figure 1: Case 22A - Present code predictions compared with experimental data and ANTICE results

Table 2: Thermal Boundary-Layer Models

	Present		Classic	
Regime	model	equation	model	equation
Laminar	Ambrok[20]	Eq. (14)	Smith and Spalding[19]	Eq. (18)
Turbulent	Ambrok[20]	Eq. (16), (17)	*Colburn* analogy	Eq. (16), (19)
Transitional	Reynolds, Kays and Kline[37]	Eq. (20), (21)	abrupt model	-

experimental data sets.[8,10] The *Colburn* momentum and heat analogy model, which assumes flow over smooth surfaces, was chosen instead of the fully rough turbulent convective heat transfer coefficient. The later is used in classic icing codes and may lead to overestimation as observed by Gent, Dart and Cansdale[6] and present authors during research of Silva.[30] In all figures, the results of the present model with transition onset and extension predictions, provided by Abu-Ghannam and Shaw correlations,[39] is identified as present+AS. A freestream turbulence level of $Tu = 0.7\%$ was adopted for all onset predictions. This is in agreement with recent measurements in NASA Icing Research Tunnel[43] for same LWC and MVD range used in present paper.

Figure 1(a) shows that the airfoil surface temperature T_{wall} distribution predicted by present model is closer to experimental data[10] than classic (isothermal plus abrupt transition) model, present with transition prediction as well as ANTICE code results. The main reason for the satisfactory accuracy obtained is that the both overall and convective heat transfer coefficient distributions are also closer to measurements, as shown in Fig. 2(a) and 1(b). The transition region parameters were arbitrarily fixed and predicted at values presented in Table 3. As done in previous works,[1–5] both s_m and σ of present model were defined by minimizing deviation of numerical results to T_{wall} and U measurements. This procedure has been adopted because the present authors did not find any procedure to estimate transition parameters in flow around ice protected airfoils under icing conditions. Then, the abrupt transition position used in classic model was set to same upper and lower side s_m values than present model. Table 3 show that present+AS model predicted more downtream s_m and smaller σ than fixed values used in present model. As the rivulets are not present in case 22A, the deviations suggests that AS correlations[39] may have limited applicability and did not find the best set of transition parameters for this case.

Table 3: Transition Region Parameters for Present Model

	Fixed				Predicted - AS model[39]			
	s/c upper		s/c lower		s/c upper		s/c lower	
	s_m	σ	s_m	σ	s_m	σ	s_m	σ
22A	0.070	0.035	−0.080	0.040	0.082	0.012	−0.084	0.012
67A	0.070	0.007	−0.067	0.007	0.066	0.010	−0.066	0.010
8 icing	0.070	0.035	−0.036	0.018	0.039	0.006	−0.039	0.006
8 clear air	0.110	0.055	−0.070	0.037	0.039	0.006	−0.039	0.006

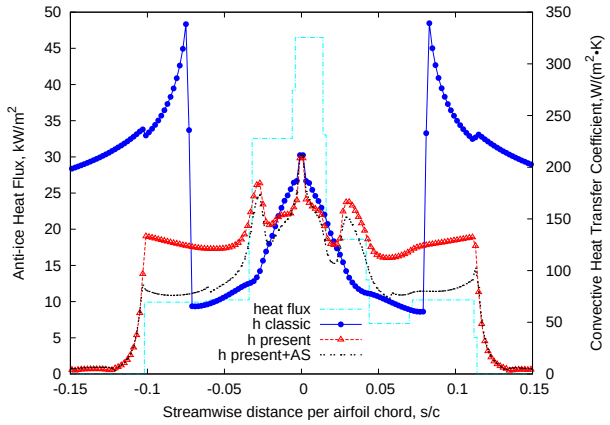

(a) Convective heat transfer coefficient and electrical power density distributions

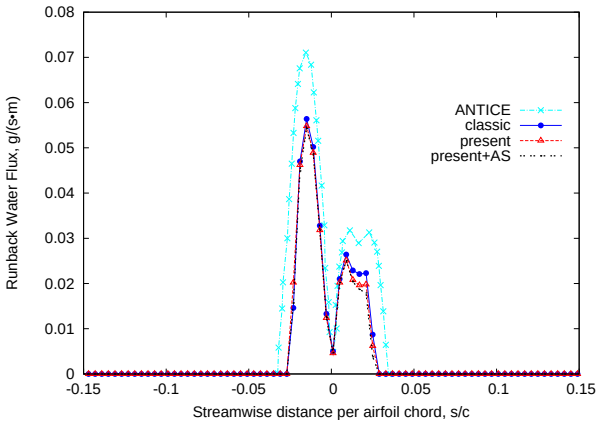

(b) Runback water

Figure 2: Case 22A - Present code predictions compared with ANTICE results

The case 22A runback distributions presented approximately same trends for all models implemented in present paper, as shown in Fig. 2(b). This may be caused by the small differences between the h_{air} predicted by the models within the impingement region, where the liquid water film still exists. On the other hand, the differences are significant when comparing h_{air} values along whole airfoil of present, present+AS and classic model presented in Fig. 2(a). The greatest discrepancies are the sharp variation of h_{air} at transition from laminar to turbulent regime and the insensitivity of h_{air} to T_{wall} streamwise variations in predictions of the classic model.

Figure 3 presents the surface temperature and heat transfer coefficients distributions around airfoil leading edge region for case 67A of Al-Khalil *et al.*[10] data set. As in the case 22A, the present model presented lower deviation between numerical predictions and experimental data than classic model, present+AS and ANTICE code, which used the experimental heat transfer distribution to calculate the T_{wall} and runback mass flux. As the surface temperatures were approximately constant, the main difference between models is observed at laminar-turbulent transition region. The approximately same laminar h_{air}, which covers from stagnation to the end of runback flow, caused very similar runback distribution for present and classic models. The difference in surface temperatures start to be significant at transition onset position, which is close to the end of rivulets flow. However, the present+AS model had different temperature results but still close to experimental data than other models because it predicted an earlier and longer transition. Table 3 presents the transition parameters adopted and predicted in case 67A. Figure 4(b) show the runback flow predicted by present, present+AS and classic models. The main differences among them are located between transition onset and end of rivulets flow. In this case, as smoother (longer and earlier) the transition is,

more downstream the runback ends.

The surface wetness factor for case 22A and 67A is presented in Figs. 5(a) and 5(b), respectively. The first has only runback flowing as a continuous film, since it ends before the impingement limits. According to models, the second presents both film, with $F = 1$, and rivulets flow patterns, which is indicated by $F < 1$ values.

Table 3 shows the transition region parameters (s_m and σ) for case 67A. The model present+AS predicted a more upstream s_m and longer transition length $4 \cdot \sigma$ than values fixed by adjustment of T_{wall} and U with experimental data in present model. The classic model uses s_m fixed in present model as the position for abrupt transition.

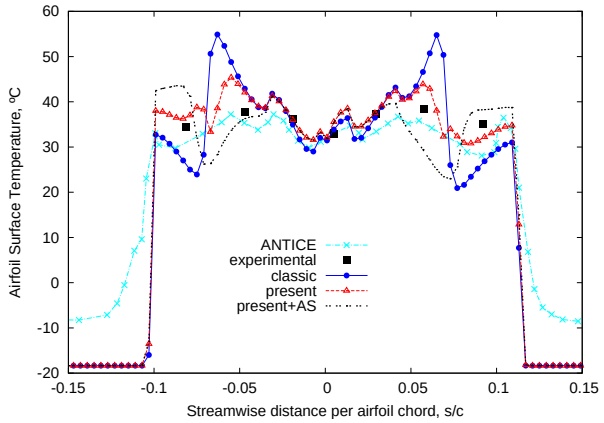

(a) Surface Temperature

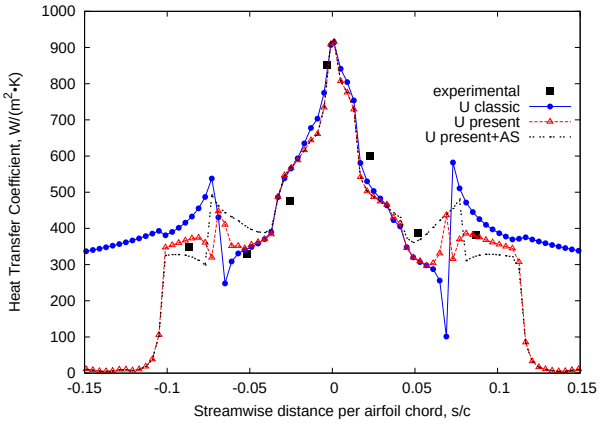

(b) Overall heat transfer coefficient

Figure 3: Case 67A - Present code predictions compared with experimental data and ANTICE results

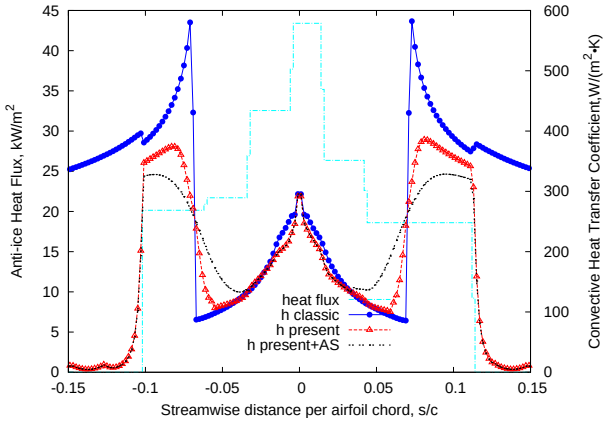

(a) Convective heat transfer coefficient and electrical power density distributions

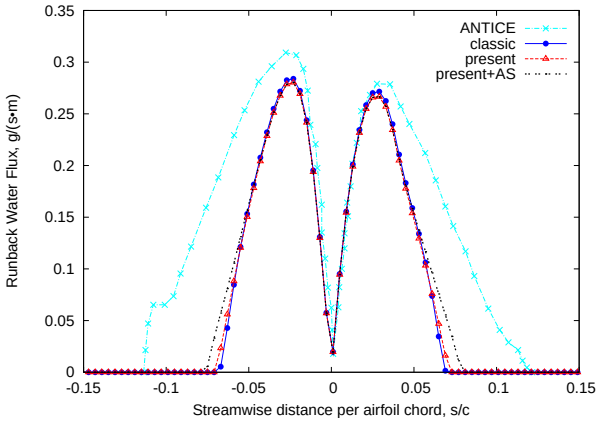

(b) Runback water

Figure 4: Case 67A - Present code predictions compared with ANTICE results

Present paper numerically simulated the classic anti-icing experiments of Gelder and Lewis.[8] This data set has not been used by researchers of icing field since long time. The data present significant surface temperature variations due to asymmetrical and non-uniform electrical heating distribution. The predicted surface temperatures for icing and clear air tests, shown respectively in Figs. 6(a) and 8(a), present deviations in relation to experimental data probably due three main reasons: 1) the authors did not have heat flux gauges installed around airfoil and measured only the electrical power provided to the heaters, thus, the thermal losses were not determined experimentally; 2) the abrupt step in heating at $s/c \approx 0.3$ caused a significant effect on experimental h_{air} that can not be reproduced neither by non-isothermal nor isothermal

models due to integral analysis intrinsic limitations; 3) temperature measurement errors in leading edge region as observed by the authors[8] during clear air flow around airfoil adiabatic surface tests.

However, the predictions, mainly upstream $s/c = 0.3$, are considered to be acceptable for ice protection system engineering purposes. The h_{air} predicted by present model agreed satisfactorily with experimental data. It matches test results better in icing, Fig. 6(b), than in clear air Fig. 8(b) condition. The only points with significant deviations were at the region of the heating step ($s/c \approx 0.3$), where the power density was suddenly increased by almost four times. Despite the disturtance of such magnitude, the present and present+AS models predicted h_{air} distribution with same trend of experimental data, including a sharp but not too intense variation of h_{air} at beginning of heating step. Both icing and clear air h_{air} and heat power density distributions are shown in Fig. 9. The runback flow and F distributions are presented in Fig. 7. They have approximately same values because the runback flow is concentrated around a narrow region around leading edge where the h_air and C_f values are similar. Table 4 shows the the runback, impingement and ice protected area limits for Gelder and Lewis[8] condition 8.

The numerical results of present model (with fixed transition), shown in Table 3 and Figures 6 and 8, are in agreement with Gelder and Lewis[8] experimental observations: 1) the laminar-turbulent transition was triggered just downstream the stagnation; 2) the onset position in icing was located more upstream than clear air condition; 3) the extension of laminar-turbulent transition region has significant effects in both cases. The present+AS model predicted a laminar-turbulent transition with shorter extension and mean position more upstream than the present and classic models, which caused a significant deviation between the numerical results and experimental data. This fact is expected since semi-empirical models like AS correlations[39] were defined based on flow over isothermal, non-heated and smooth surfaces without droplets impingement, evaporation and runback water flow. The different disturbancies, which are found in flow around airfoils operating icing tunnels, may trigger different unstability mechanisms and cause the laminar-turbulent transition to follow other routes not comprised by the semi-empirical correlations.

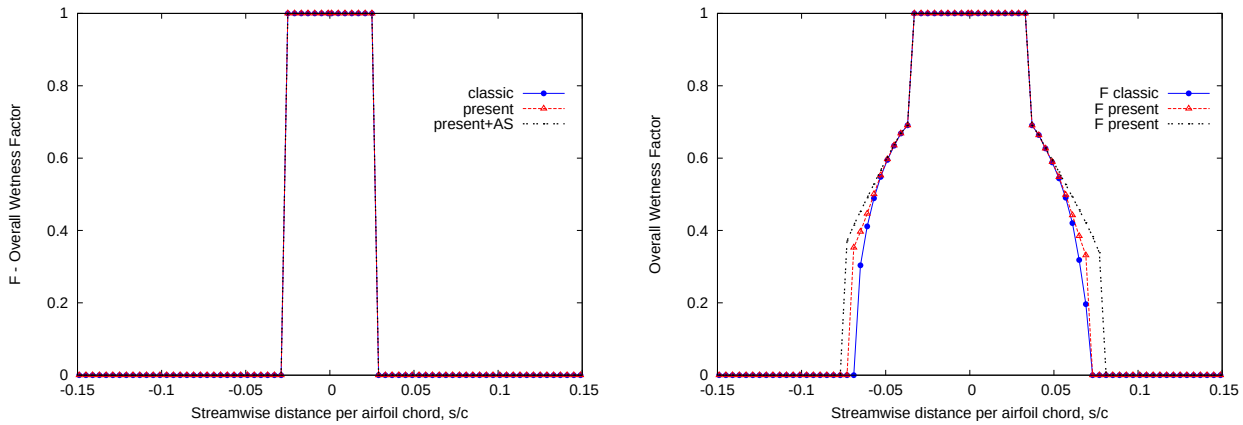

(a) Case 22A (b) Case 67A

Figure 5: Present code predictions for overall wetness factor - F

X. Conclusions

The heated airfoil operating under icing conditions has some important characteristics that differentiates the problem from the case of adiabatic airfoil subjected to ice growth. In presence of thermal ice protection, the boundary-layer flow over isothermal surfaces hypothesis assumed by most classic icing codes may not represent the operation adequately. The streamwise surface temperature gradient, water evaporation rate variation and the occurrence of transition, within the protected area, are effects that must be represented adequately by the mathematical models.

Prediction improvements were noticed at laminar-turbulent transition region, end of water flow positions, high streamwise temperature gradient regions, abrupt heating steps, end of thermally protected area and wet regions, where the airfoil surface is fully (continuous film) or partially (rivulets) covered by water flow. Particularly in wet cases, the present work concluded that laminar-transition transition occurrence is the

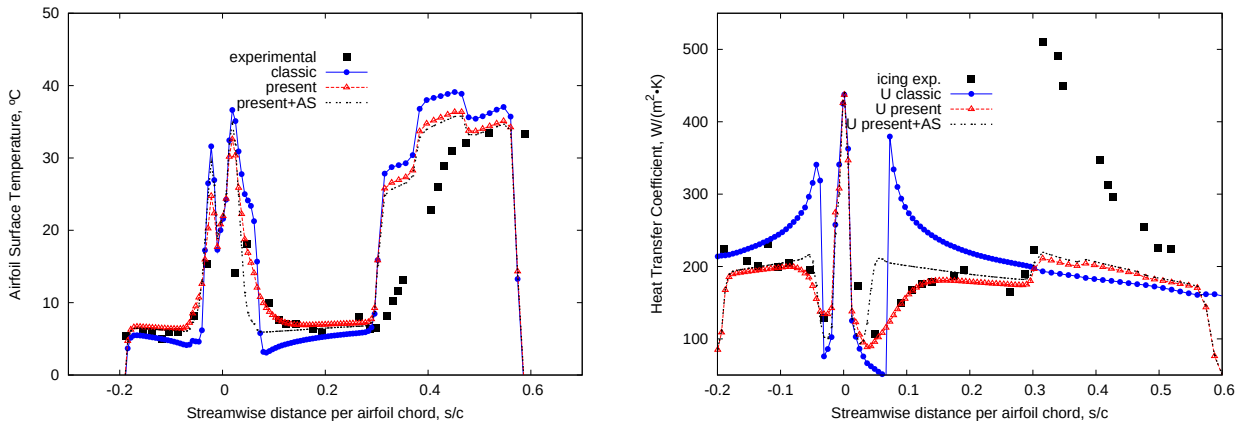

(a) Surface Temperature

(b) Overall heat transfer coefficient

Figure 6: Icing condition 8 - Present code predictions compared classic experimental data

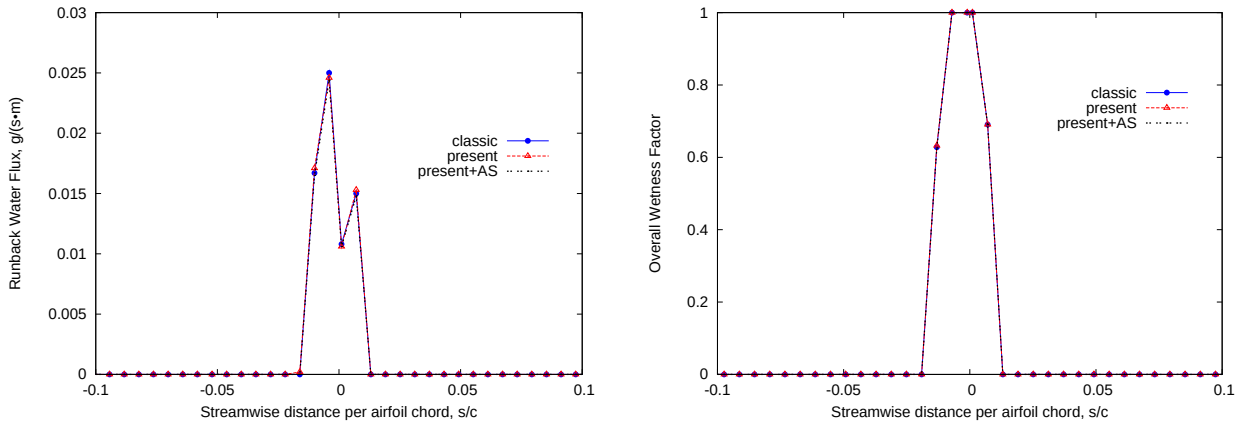

(a) Runback water flux

(b) Overall wetness factor

Figure 7: Icing condition 8 - Runback and surface wetness predictions

most significant effect that affects heat transfer coefficient, surface temperature and water evaporation.

A laminar-turbulent transition region may occur within the airfoil thermal protected region. Depending on the onset position and length of transition region, the laminar flow may cover a significant area when compared to fully turbulent flow area and vice-versa. The assumption of preponderance of one regime over another (only laminar or only turbulent approximation) will lead to a inadequate mean heat transfer coefficient prediction along the heated area. Moreover, an abrupt local heat transfer coefficient variation from laminar to turbulent value causes great impact in local parameters such as the surface temperature, evaporation mass flux distributions as well as the position where the liquid water disappears. In this case, a local parameter prediction is much more sensitive to transition occurrence than an integral parameter that is averaged over a surface.

Therefore, the history convective heat transfer coefficient is important to thermal ice protection simulation. Variations in flow parameters, surface thermo-mechanical disturbancies and transition occurrence may produce variations in heat transfer coefficient that will generate impacts on the temperature and runback local values around thermally protected aifoils.

It is recommended to be attentive when using classical semi-empirical criteria, such as the one analyzed herein, or other automated procedures to predict the onset and length of transition region. These procedures may have a limited validity range and, therefore, not be applicable to predict transition parameters of flows around heated airfoils under natural ice flight or icing tunnel conditions.

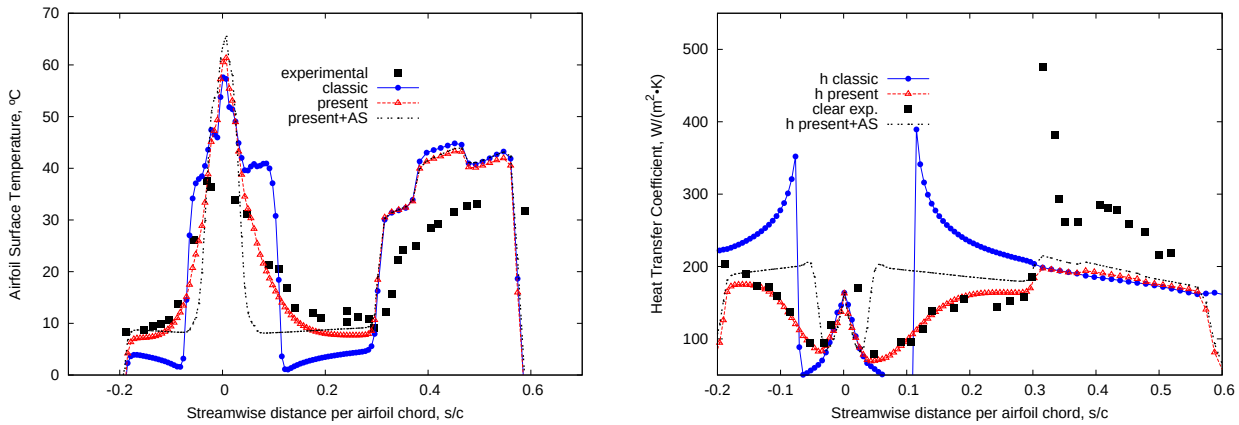

(a) Surface Temperature

(b) Overall heat transfer coefficient

Figure 8: Clear air condition 8 - Present code predictions compared with classic experimental data

Table 4: Runback Flow, Impingement and Ice Protected Area Limits

		s/c upper side			s/c lower side		
Case	model	runback	impingement	heaters	runback	impingement	heaters
22A	present.	0.024	0.031	0.113	−0.026	−0.031	−0.102
	classic	0.024			−0.024		
	present+AS	0.025			−0.025		
67A	present.	0.069	0.037	0.113	−0.069	−0.037	−0.102
	classic	0.071			−0.069		
	present+AS	0.079			−0.075		
8	present.	0.101	0.071	0.576	−0.131	−0.131	−0.190
	classic	0.101			−0.131		
	present+AS	0.101			−0.131		

Finally, the use of a classic experimental data set, which has not been used for numerical code validation purposes in recent literature, reaffirm the validity of those experiments, verify applicability of the present numerical tool and may demonstrate the robustness of the mathematical model to represent the physical phenomena.

Acknowledgment

One of authors (G. A. L. da Silva) wishes to acknowledge Fundação de Amparo à Pesquisa do Estado de São Paulo (FAPESP) for the financial support received by the doctoral grant 07/00419-0.

References

[1]Silva, G. A. L., Silvares, O. M., and Zerbini, E. J. G. J., "Airfoil anti-ice system modeling and simulation," *AIAA Paper 2003-734*, Aerospace Sciences Meeting and Exhibit, 43., 2005, Reno, America Institute of Aeronautics and Astronautics, Reston, 2003.

[2]Silva, G. A. L., Silvares, O. M., and Zerbini, E. J. G. J., "Simulation of an Airfoil Electro-Thermal Anti-Ice System Operating in Running Wet Regime," *AIAA Paper 2005-1374*, Aerospace Sciences Meeting and Exhibit, 41., 2003, Reno, American Institute of Aeronautics and Astronautics, Reston, Janeiro 2005.

[3]Silva, G. A. L., Silvares, O. M., and Zerbini, E. J. G. J., "Water Film Breakdown and Rivulets Formation Effects on Thermal Anti-ice Operation Simulation," *AIAA Paper 2006-3785*, AIAA/ASME Joint Thermophysics and Heat Transfer

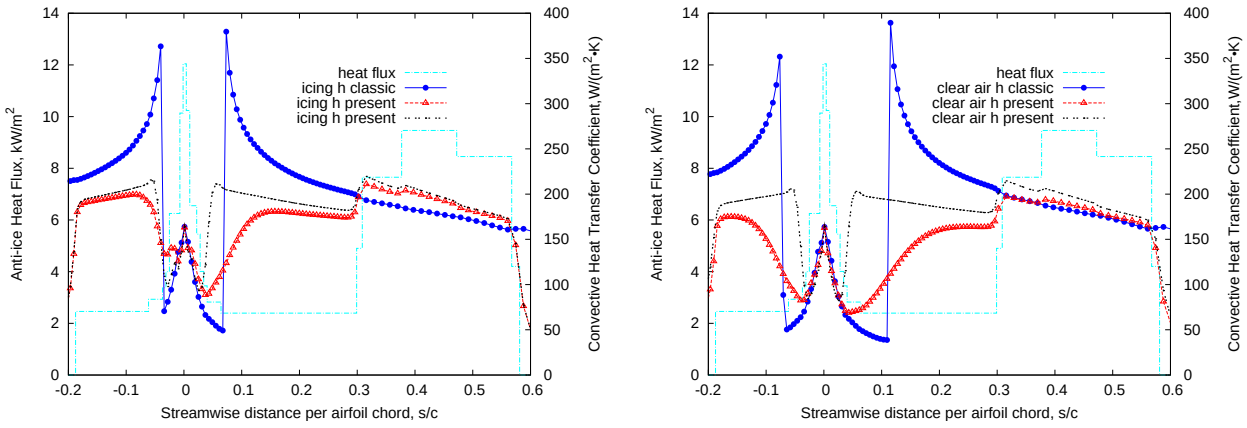

(a) Icing (b) Clear air

Figure 9: Condition 8 - Convective heat transfer coefficient and electrical power density distributions

Conference, 9., 2006, San Francisco, America Institute of Aeronautics and Astronautics, Reston, June 2006.

[4]Silva, G. A. L., Silvares, O. M., and Zerbini, E. J. G. J., "Numerical Simulation of Airfoil Thermal Anti-ice Operation. Part 1: Mathematical Modeling," *Journal of Aircraft*, Vol. 44, No. 2, March-April 2007, pp. 627–33.

[5]Silva, G. A. L., Silvares, O. M., and Zerbini, E. J. G. J., "Numerical Simulation of Airfoil Thermal Anti-ice Operation. Part 2: Implementation and Results," *Journal of Aircraft*, Vol. 44, No. 2, March-April 2007, pp. 634–41.

[6]Gent, R. W., Dart, N. P., and Cansdale, J., "Aircraft Icing," *Phil. Trans. Royal Society London A*, , No. 358, 2000, pp. 2873–2911.

[7]Stefanini, L. M., Silvares, O. M., Silva, G. A. L., and Zerbini, E. J. G. J., "Convective Heat Transfer Effects in Airfoil Icing," *Procedings of COBEM 2007*, 19th International Congress of Mechanical Engineering, Brazilian Society of Mechanical Sciences and Engineering, Rio de Janeiro, November 2007, Submitted for publication.

[8]Gelder, T. F. and Lewis, J. P., *Comparison of heat transfer from airfoil in natural and simulated icing conditions*, National Advisory Committee for Aeronautics, Washington, September 1951, 52 p. (Technical Note, 2480).

[9]Sogin, H. H., *A design manual for thermal anti-icing systems*, Wright Air Development Center Technical, Illinois, 1954, (Technical Report, 54-13).

[10]Al-Khalil, K. M., Horvath, C., Miller, D. R., and Wright, W., *Validation of NASA thermal ice protection computer codes. Part 3 - Validation of ANTICE*, National Aeronautics and Space Agency, Cleveland, OH, May 2001, 18 p. (Contractor Report, 2001-210907).

[11]Gent, R., Moser, R., Cansdale, J., and Dart, N., "The Role of Analysis in the Development of Rotor Ice Protection System," *SAE Paper 2003-01-2090*, FAA In-flight Icing, Ground De-icing International Conference & Exhibition, 1., Chicago, 2003, IL, Society of Automotive Engineers, Warrendale, June 2003.

[12]Makkonen, L., "Heat Transfer and icing of a rough cylinder," *Cold Regions and Technology*, Vol. 10, 1985, pp. 105–116.

[13]Wright, W. B., *User Manual for the Improved NASA Lewis Ice Accretion Code LEWICE 1.6*, National Aeronautics and Space Administration, Cleveland, May 1995, 95 p. (Contractor Report, 198355).

[14]Guffond, D. and Brunet, L., *Validation du programme bidimensionnel de capitation*, Office National D'Études et de Recherches Aérospatiales, Châtillon Cedex, France, 1988, (Rapport Technique , RP 20/5146 SY).

[15]Gent, R., *TRAJICE2 - A Combined Water Droplet Trajectory and Ice Accretion Prediction Program For Aerofoils*, Royal Aerospace Establishment, Farnborough, 1990, (Technical Report, 90054).

[16]Wright, W., Gent, R., and Guffond, D., *DRA/NASA/ONERA Collaboration on Icing Research Part II - Prediction of Airfoil Ice Accretion*, National Aeronautics and Space Administration, Cleveland, May 1997, 50 p. (Contractor Report,202349).

[17]Wright, W. B., *User Manual for the NASA Glenn Ice Accretion Code LEWICE Version 2.0*, National Aeronautics and Space Administration, Cleveland, 1999, 181 p. (Contractor Report, 209409).

[18]Morency, F., Tezok, F., and Paraschivoiu, I., "Heat and Mass Transfer in the Case of an Anti-icing System Modelisation," *AIAA Paper 99-0623*, Aerospace Sciences Meeting and Exhibit, 37., 1999, Reno, American Institute of Aeronautics and Astronautics, Reston, Janeiro 1999.

[19]Smith, A. G. and Spalding, D. B., "Heat transfer in a laminar boundary layer with constant fluid properties and constant wall temperature," *Journal of the Royal Aeronautical Society*, Vol. 62, 1958, pp. 60–64.

[20]Ambrok, G. S., "Approximate Solution of Equations for the Thermal Boundary Layer with Variations in Boundary Layer Structure," *Soviet Physics - Technical Physics*, , No. 2, 1957, pp. 1979–86.

[21]Henry, R., *Etude du fonctionnement d'un degivreur electrique : modelisation et mesure en soufflerie givrante de temperature parietale par thermographie infrarouge*, Ph.D. thesis, Blaise Pascal Université, Clemont-Ferrand, 1989.

[22]Cebeci, T. and Bradshaw, P., *Physical and Computational Aspects of Convective Heat Transfer*, Springer-Verlag, New York, 1984.

[23]Cebeci, T., *Effects of environmentally imposed roughness on airfoil performance*, National Aeronautics and Space Administration, Washington, June 1987, 48 p. (Contractor Report, 179639).

[24]Cebeci, T., "Calculation of Flow Over Iced Airfoils," *Journal of Aircraft*, Vol. 27, No. 7, Junho 1989, pp. 853–61.

[25]Cebeci, T., Chen, H. H., and Alemdaroglu, N., "Fortified LEWICE with Viscous Effects," *Journal of Aircraft*, Vol. 28, No. 9, Setembro 1991, pp. 564–71.

[26]Cebeci, T., Chen, H. H., Kaups, K., Schimke, S., and Shin, J., *Analysis of Iced Wings*, National Aeronautics and Space Administration, Washington, January 1992, 16 p. (Technical Memorandum, 105773).

[27]Henry, R., *Development of an electrothermal de-icing/anti-icing model*, Office National d'Etudes et de Recherches Aérospatiales, Chatillon Cedex, 1992, (Rapport ONERA TAP, 92005).

[28]Morency, F., Tezok, F., and Paraschivoiu, I., "Anti-icing System Simulation Using CANICE," *Journal of Aircraft*, Vol. 36, No. 6, 1999.

[29]Croce, G., Beaugendre, H., and Habashi, W., "CHT3D: Fensap-Ice Conjugate Heat Transfer Computations With Droplet Impingement And Runback Effects," *AIAA Paper 2002-0386*, Aerospace Sciences Meeting & Exhibit 40., 2002, Reno, America Institute of Aeronautics and Astronautics, Reno, Nevada, January 2002, pp. 1–10.

[30]Silva, G. A. L., *Modelagem e simulação da operação de sistema antigelo eletrotérmico de um aerofólio*, Master's thesis, Escola Politécnica da Universidade de São Paulo, São Paulo, SP, Brazil, April 2002.

[31]Domingos, R. H., Pustelnik, M., Trapp, L. G., Silva, G. A. L., Campo, W., and Santos, L. C. C., "Development of an Engine Anti-ice Protection System using Experimental and Numerical Approaches," *SAE paper 2007-01-3355*, SAE Aircraft and Engine Icing International Conference, 2007, Seville, Society of Automotive Engineers., Warrendale, September 2007, Accepted for publication.

[32]Spalding, D. B., *Convective mass transfer, an introduction*, McGraw-Hill, New York, 1963.

[33]Mikielewicz, J. and Moszynski, J. R., "Breakdown of a shear driven liquid film," *Polzka Akademia Nauk. - Prace Instytutu Maszyn Przeplywowych*, , No. 66, 1975, pp. 3–11.

[34]Mikielewicz, J. and Moszynski, J. R., "Minimum thickness of a liquid film flowing vertically down a solid surface," *Int. J. Heat and Mass Transfer*, Vol. 19, 1976, pp. 771–776.

[35]Kays, W. M. and Crawford, M. E., *Convective heat and mass transfer*, McGraw-Hill, New York, 1993.

[36]Thwaites, B., "Approximate Calculation of the Laminar Boundary Layer," *Aero. Quart.*, Vol. 10, 1949, pp. 245–79.

[37]Reynolds, W. C., Kays, W. M., and Kline, S. J., *Heat transfer in the turbulent incompressible boundary layer. IV - Effect of location of transtion and prediction of heat transfer in a known transition region*, National Aernautics and Space Administration, Washington, D.C., December 1958, (Memorandum, 12-4-58W).

[38]Narasimha, R., *Modelling the transitional boundary layer*, National Aernautics and Space Administration, Washington, 1990, 30 p. (Contractor Report, 187487).

[39]Abu-Ghannam, B. and Shaw, R., "Natural Transition of Boundary Layers - The Effects of Turbulence, Pressure Gradient and Flow History," *Journal of Mechanical Engineering Science*, Vol. 22, No. 5, 1980, pp. 213–228.

[40]Pimenta, M. M., *The turbulent boundary layer: an experimental study of the transport of momentum and heat with the effects of roughness*, Ph.D. thesis, Stanford University, Stanford, May 1975.

[41]Bragg, M. B., Cummings, S. L., and Henze, C. M., "Boundary-layer and heat transfer measurements on an airfoil with simulated ice roughness," *AIAA Paper 96-0866*, Aerospace Sciences and Meeting, 34., 1996, Reno, America Institute of Aeronautics and Astronautics, Reston, January 1996, pp. 1–16.

[42]Neel, Junior, C. B. and Bergrun, N. R., *The calculation of the heat required for wing thermal ice prevention in specified icing conditions*, National Advisory Committee for Aeronautics, Washington, September 1947, (Technical Note, 1472).

[43]Henze, C., Bragg, M., and Kim, H., "Freestream Turbulence Measurements in Icing Conditions," *AIAA-1998-96*, AIAA, Reno, January 1998.